Maximizing the visible light photoelectrochemical activity of B/N-doped anatase TiO_2 microspheres with exposed dominant {001} facets

Xingxing Hong,[1,2] Yuyang Kang,[1,2] Chao Zhen,[1] Xiangdong Kang,[1] Li-Chang Yin,[1] John TS Irvine,[3] Lianzhou Wang,[4] Gang Liu,[1,2,*] Hui-Ming Cheng[1,5,6,]

[1]Shenyang National Laboratory for Materials Science, Institute of Metal Research, Chinese Academy of Sciences, 72 Wenhua Road, Shenyang 110016, China

[2]School of Materials Science and Engineering, University of Science and Technology of China, 72 Wenhua Road, Shenyang 110016, China

[3]School of Chemistry, University of St. Andrews, Fife, KY16 9ST, UK

[4]Nanomaterials Centre, School of Chemical Engineering and AIBN, The University of Queensland, St Lucia, Brisbane, QLD 4072, Australia

[4]Tsinghua-Berkeley Shenzhen Institute, Tsinghua University, 1001 Xueyuan Road, Shenzhen 518055, China

[6]Center of Excellence in Environmental Studies, King Abdulaziz University, Jeddah 21589, Saudi Arabia

Correspondence and requests for materials should be addressed to G.L. (email: gangliu@imr.ac.cn)

Abstract

Anatase TiO_2 spheres with exposed dominant {001} facets were doped with interstitial boron to have a concentration gradient with the maximum concentration at the surface. They were then further doped with substitutional nitrogen by heating in an ammonia atmosphere at temperatures from 440 to 560 °C to give surface N concentrations ranging from 7.03 to 15.47 at%. The optical absorption, atomic and electronic structures and visible-light photoelectrochemical water oxidation activity of these materials were investigated. The maximum activity of the doped TiO_2 was achieved at a nitrogen doping temperature of 520 ^oC that gave a high absorbance over the whole visible light region but with no defect-related background absorption.

Introduction

Solar energy is the most abundant renewable energy source for mankind and is considered to play a very important role in constructing environmentally-friendly energy supply systems. Among the various modern technologies for using solar energy, photocatalysis represents an amazing route of simultaneously converting and storing solar energy in the form of chemical energy by inducing targeted redox reactions such as water-splitting to release hydrogen and reduce carbon dioxide to produce high-value chemicals on the photocatalyst surface. Since the pioneering work on photoelectrochemical water splitting using a rutile TiO_2 single crystal as photoanode,[1] intensive studies over 40 years, particularly in the last decade, have achieved substantial developments in photocatalysis.[2-9] Specifically, overall water-splitting on the basis of a solid-state Z-scheme system of La/Rh codoped $SrTiO_3$/Au/Mo doped $BiVO_4$ sheets doped with both La and Rh gave a solar-to-hydrogen energy conversion efficiency of over 1%.[10] In addition, photocatalytic water-splitting under irradiation with 600 nm visible light was achieved on a complex metal oxynitride photocatalyst, although its quantum efficiency was still low.[11] The impressive progress strongly demonstrates the great promise of solar-driven photocatalysis in converting solar energy into storable chemical energy.

Compared to the rapid development of complex metal oxide photocatalysts,[5, 12] making the simple binary photocatalyst TiO_2 active so that it can fully harvest visible light is a challenge.[13-22] TiO_2 is easily available and low-cost, but has no visible light absorption due to its large bandgap of around 3 eV. Introducing suitable heteroatoms to

replace Ti and/or O atoms in it has shown the feasibility of increasing visible light absorption. Among many possible doping strategies, substitutional N-doping (N atom substituting lattice O atom) has been supposed to be able to lift the valence band maximum of TiO_2 due to the higher orbital energy levels of N-2*p* than those of O-2*p*. Unfortunately, N-doping is highly limited as a result of low solubility and inhomogeneous distribution in most metal oxides with strong metal-oxygen bonds. [23-25]. In the case of TiO_2, this can only introduce some localized states of dopants in the band gap and give rise to a low absorbance of the extended visible light absorption band. Our previous study[25] showed that interstitial boron in anatase TiO_2 can greatly weaken the strong Ti-O bonds to facilitate the replacement of oxygen with nitrogen. In the subsequent nitrogenation process, the boron concentration gradient in the TiO_2 resulted in a nitrogen concentration gradient in a red B/N doped anatase TiO_2 photocatalyst with a strong absorption band in the spectrum of visible light. Moreover, charge compensation between the boron and nitrogen dopants suppresses the formation of deleterious recombination centers of charge carriers. In contrast to this red TiO_2 with a high concentration of nitrogen dopant, regular nitrogen-doped TiO_2 showed a photocatalytic activity decrease with an increase of nitrogen dopant.[26] Research on the dependence of the photocatalytic activity of red TiO_2 on the concentration of nitrogen dopant and its mechanism at the electronic level should provide useful guidelines to the development of both red TiO_2 and other binary metal oxide photocatalysts.

In this study, the concentration of nitrogen dopant in red TiO_2 photocatalysts was

increased by increasing the nitrogenation temperature from 440 ºC to 560 ºC and its effect on photoelectrochemical water oxidation activity was studied. Several characterization methods were used to understand why there was a maximum activity at an optimum surface nitrogen concentration.

Results

The morphology and microstructure of representative B/N doped anatase TiO_2 microspheres were studied by scanning (SEM) and transmission electron microscopy (TEM), as shown in Figure 1. The microsphere surface consists of dominant square {001} facets with an edge size of tens of nanometers and minor {101} facets. The obtuse angle between {001} and {101} facets measured in Fig. 1c is around 111.7º, which is a good match with the ideal crystallographic value.[28] Additional N-doping did not change the basic shape of the microspheres. However, compared to the sharp edges of the square {001} facets of the pristine boron-doped TiO_2 microspheres (Fig. S5 of reference 27), the edges those further doped with N were less defined as a result of the nitrogen diffusion from the surface to the bulk. A high resolution TEM image (Fig. 1d) shows lattice fringes of (001) planes with a spacing of 2.4 Å. Unclear fringes also suggest some disruption of the local atomic structure as a result of the introduction of a high concentration of nitrogen.

The chemical states and concentrations of nitrogen and boron dopants in different boron/nitrogen doped TiO_2 samples prepared at the different nitrogenation temperatures were investigated by X-ray photoelectron spectroscopy (XPS), and the results are given

in Figure 2. The pristine boron-doped TiO_2 has interstitial boron with a B 1*s* core electron binding energy of 192.2 eV indicating the presence of B-O bonds. With the introduction of nitrogen dopant, an additional B 1*s* XPS signal with a binding energy around 190.3 eV was formed due to the formation of B-N bonds.[25] The ratio of boron in B-N bonds to that in B-O bonds in the sample obtained at a temperature of 440 ºC is 0.52 due to the low concentration of the nitrogen dopant and increases to 1.28 for the 560 ºC sample (determined from the area ratio of XPS B 1*s* peaks in B-O and B-N bonds). This is the result of the increased nitrogen content that is indicated by the stronger XPS peak of N 1*s* core. The oxidation state of the dominant nitrogen species (N 1*s*, binding energy 397.6 eV) in the sample is very close to that in TiN or Ti-N bonds,[13] suggesting the substitution of nitrogen for oxygen in the TiO_2. The unchanged binding energy of the nitrogen species in different samples demonstrates the independence of its oxidation state on the nitrogenation temperature. Note that the minor fitted peak centered at 399.3 eV is assigned to interstitial nitrogen. It seems that, on the basis of the evolution of the peaks of the two different nitrogen species, high temperature nitrogenation favors the incorporation of substitutional rather than interstitial nitrogen. Moreover, the atomic ratio of nitrogen to titanium increases from 7.03% at 440 ºC to 15.47% at 560 ºC (the values for each temperature are given in **Table S1**). It should be pointed out that the nitrogen concentration given here directly reflects the situation in several nanometer thick surface layer of the microspheres due to surface sensitivity of XPS technique itself.

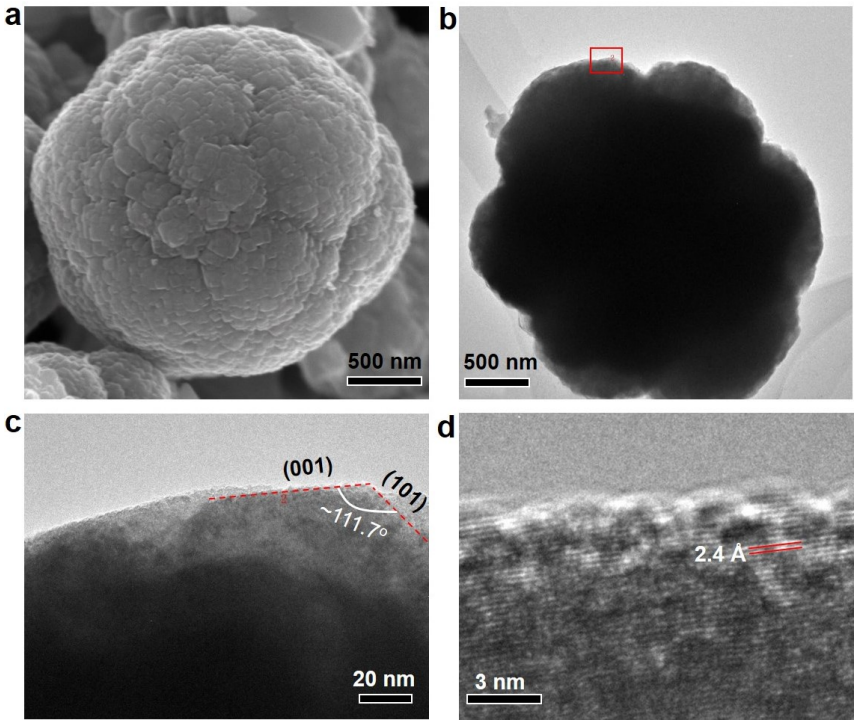

Figure 1 a and **b,** SEM and TEM images of a representative N/B-doped anatase TiO_2 microsphere with the top surface consisting of {001} facets prepared by heating pristine boron-doped anatase microspheres at 520 ºC in a gaseous ammonia atmosphere. **c** and **d**, high resolution TEM images showing the exposed top {001}/{101} facets, recorded from the region marked by the red rectangle in Figure 1b.

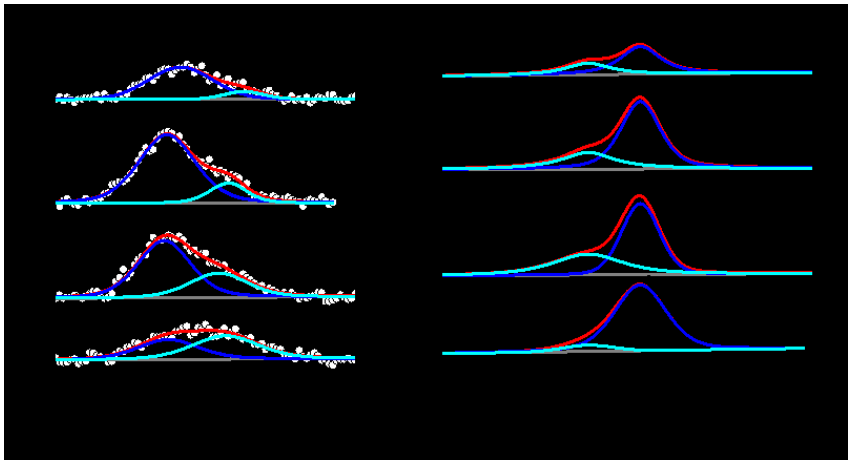

Figure 2 Representative X-ray photoelectron spectra of B 1s and N 1s core electrons recorded from the pristine surface of the B/N doped TiO_2 microspheres prepared at the different nitrogenation temperatures (440 ºC, 480 ºC, 520 ºC and 560 ºC).

The close dependence of the optical absorption band of B/N-doped TiO_2 on the nitrogenation temperature was detected by UV-visible absorption spectroscopy (Figure 3). Two features are seen in Figure 3a. 1) An additional shoulder-like absorption band spanning the whole spectrum of visible light is formed after the incorporation of nitrogen at 440 ^oC. The absorption of this visible light band gradually increases with increasing amounts of nitrogen dopant at higher nitrogenation temperatures. 2) No obvious background absorption in the wavelength range beyond 700 nm is formed for the three samples obtained at temperatures $\leq$ 520 ^oC while a strong featureless background absorption band beyond 700 nm is formed for the TiO_2-560 sample.

The first feature can be understood as follows. The origin of the visible light absorption band is the newly formed N 2*p* states with a higher energy level than the pristine O 2*p* dominated valence band edge of TiO_2. The dispersion width of N 2*p* states increases with both the concentration and spatial distribution of substitutional nitrogen in TiO_2 as illustrated in Figure 4. A low concentration of nitrogen located in the thin surface layer only contributes to some localized N 2*p* states in the bandgap that are responsible for the small shoulder-like absorption band, as in sample TiO_2-440 (Figure 4a).[26] A medium concentration in the relatively thick surface layer induces the formation of an isolated narrow band of main N 2*p* states above the pristine valence band that is responsible for a large shoulder-like absorption band seen in e.g. TiO_2-480 (Figure 4b). A high N concentration in a sufficiently thick layer results in real bandgap narrowing by mixing the N 2*p* states with the pristine valence band to elevate the band edge for the desired band-to-band redshift of the absorption edge, probably as in sample

TiO_2-560 (Figure 4c).[23, 24] In contrast, the intrinsic bandgap remains basically unchanged in these two conditions (Figure 4a and b). The plots of the transformed Kubelka–Munk function against the light energy for different samples in Figure 3b further support the above analysis. The extrapolated edge of the visible light absorption band of sample TiO_2-520 is 1.90 eV. The second feature is actually controlled by the formation of Ti^{3+} defects from the charge imbalance between O^{2-} and N^{3-}, which is normally observed in common N-doped TiO_2.[26] The presence of the interstitial boron with additional donor electrons suppresses the formation of Ti^{3+} by forming B-N bonds (Figure 2). However, the very high concentration of nitrogen introduced in sample TiO_2-560 exceeds the capability of the boron in maintaining the charge balance so that some defect states below the TiO_2 conduction band are formed.

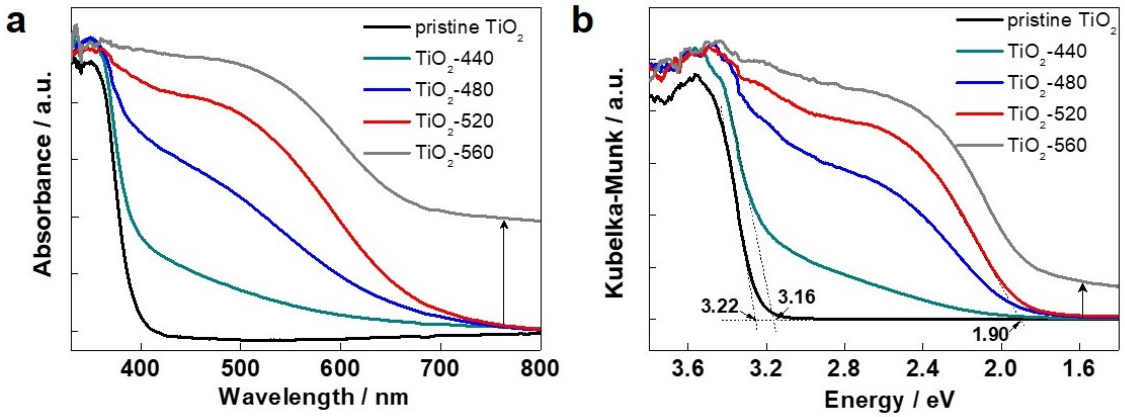

Figure 3 a, UV-visible absorption spectra of the samples of B/N-doped TiO_2 microspheres prepared at different nitrogenation temperatures (440 °C, 480 °C, 520 °C and 560 °C) compared to the pristine TiO_2 sample. **d,** corresponding plots of the transformed Kubelka–Munk function against light energy for the different samples.

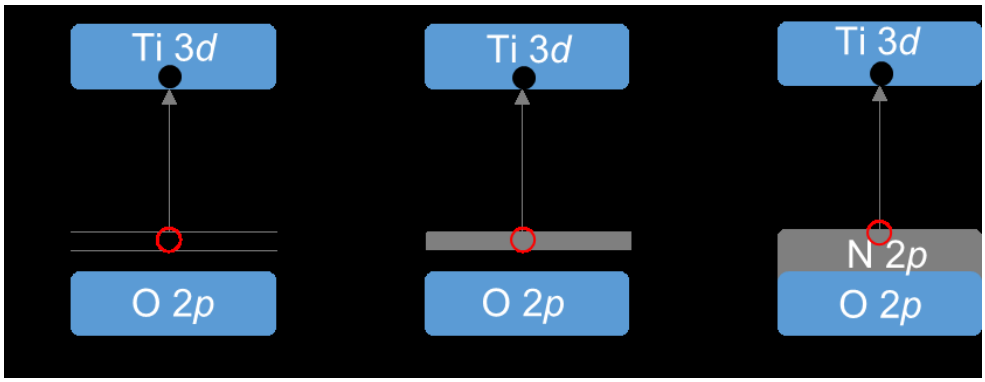

Figure 4 Schematic of the band structures of substitutional nitrogen-doped TiO_2 (containing interstitial boron) with different concentrations of nitrogen dopant: **a**, the formation of localized N 2*p* states at a low concentration of nitrogen dopant in a thin layer; **b**, the formation of an isolated narrow N 2*p* band at a medium concentration of nitrogen dopant in a relatively thick layer; **c**, bandgap narrowing at a high enough concentration of nitrogen dopant in a thick layer. CB: conduction band; VB: valence band. The pristine conduction and valence bands are dominated by Ti 3*d* and O 2*p* states, respectively.

Comparison of the absorption spectra of B/N doped TiO_2 with that of layer-structure $Cs_{0.68}Ti_{1.83}O_4$ homogeneously doped with nitrogen (Figure 1B of reference 29) where the N/Ti atomic ratio ranges from 1.09% to 16.94%),[29] reveals distinctly different changes in the additional visible light absorption band caused by nitrogen doping. The B/N doping results in a nearly identical light absorption onset at around 750 nm but gradually increased absorbance with an increase in nitrogen content. In contrast, homogeneous N doping in $Cs_{0.68}Ti_{1.83}O_4$ results in almost the same absorbance but a gradual band-to-band redshift of the light absorption onset in samples with increasing nitrogen dopant. Moreover, the nature of such a band-to-band redshift is independent

of N concentration in the case of homogeneous N doping. The distinct optical absorption modes caused by nitrogen doping can be understood in terms of the different spatial distributions and concentrations of nitrogen dopant in the TiO_2 and $Cs_{0.68}Ti_{1.83}O_4$. In principle, narrowing the bandgap of a semiconductor by doping requires the involvement of introduced heteroatoms in the strong uniform interaction field of long-range ordered intrinsic lattice atoms. For the homogeneous doping, the uniform distribution of N dopant throughout the whole particles, which is kinetically controlled by the layered structure of $Cs_{0.68}Ti_{1.83}O_4$, can meet this requirement for bandgap narrowing. The concentration of N, which is thermodynamically controlled by the nitrogenation temperature, determines the extent of the bandgap narrowing and thus the absorption onset by changing the dispersion width of N 2*p* states. For a doping gradient, the gradual decrease of N dopant concentration from the top surface to zero in the bulk leads to an inhomogeneous atomic interaction along the direction of the concentration gradient. The features of the interstitial boron-assisted substitutional nitrogen doping process in terms of both the concentration and spatial distribution of nitrogen dopant are thermodynamically controlled by the nitrogenation temperature. Low-temperature nitrogenation results in a higher concentration of nitrogen in boron-doped TiO_2 for a maximum absorption onset compared to that in layered $Cs_{0.68}Ti_{1.83}O_4$ (for example, N/Ti 7.03% in TiO_2 at 440 ^oC *vs* 1.09% in $Cs_{0.68}Ti_{1.83}O_4$ at 500 ^oC). However, the diffusion length in non-layered TiO_2 at low nitrogenation temperatures is limited so that the involvement of nitrogen in the strong long-range interaction of intrinsic lattice atoms is not enough to induce bandgap narrowing. A higher nitrogenation temperature

favors both substitutional nitrogen doping and diffusion of nitrogen from surface to bulk for the desired bandgap narrowing.

In addition to the substantial changes in the optical absorption band caused by nitrogen doping in boron-doped TiO_2, the local atomic structure was also modulated as revealed in Raman and Fourier transform infrared (FTIR) spectra. Anatase TiO_2 has six Raman active modes, $3E_g + 2B_{1g} + A_{1g}$,[30] where one of the two B_{1g} modes is hard to distinguish from the A_{1g} mode at around 515 cm^{-1} **(Fig. 5)**. Compared to the pristine boron-doped TiO_2, further nitrogen doping conducted at different temperatures shows the unchanged Raman shifts of B_{1g}, $E_{g(2)}$ and $E_{g(3)}$. However, the $E_{g(1)}$ mode seen in TiO_2-520 and TiO_2-560 shows an upshift in wavenumber from 144 to 146 cm^{-1}. Moreover, the doublet of the $B_{1g} + A_{1g}$ modes at around 515 cm^{-1} is split into two separate modes centered at 514 cm^{-1} and 494 cm^{-1}. The splitting of such a doublet can be observed at low temperature.[31] In the current case, the incorporation of a high concentration of nitrogen heteroatom into the framework of TiO_2 changes the force constants of Ti-O bonds to induce the splitting of the doublet. In contrast, most nitrogen doped TiO_2 did not show such splitting probably because the low concentration of nitrogen dopant and also surface distribution of nitrogen dopant. The shift by around 20 cm^{-1} of the fingerprint region of TiO_2 below 1000 cm^{-1} towards a low wavenumber in the FTIR spectra at the high concentration of nitrogen doping in **Figure S2** supports the local structure modulation caused by nitrogen doping. Note that the signal with the peak at 3446 cm^{-1} assigned to surface hydroxyl groups and adsorbed water molecules [32, 33] shows a negligible intensity change, suggesting good retention of the surface

hydrophilicity of TiO_2 upon nitrogen doping.

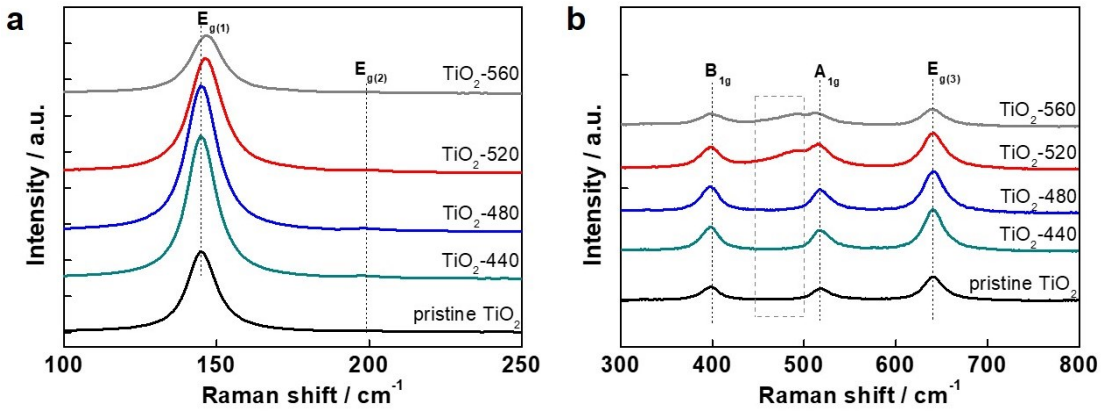

Figure 5 Raman spectra of B/N-doped TiO_2 microspheres prepared at different nitrogenation temperatures (440 °C, 480 °C, 520 °C and 560 °C) compared to the pristine boron-doped TiO_2 sample. The wavelength of the excitation light is 633 nm.

The dependence of the concentration of nitrogen dopant on the photocatalytic activity of the B/N-doped TiO_2 obtained above was studied by recording the photoelectrochemical water oxidation behavior of the TiO_2 based photoanodes under visible light irradiation (> 420 nm). Nitrogen doping greatly increases the photocurrent of the doped TiO_2 photoanodes as a result of visible light absorption. The photocurrent density increases monotonically with increased nitrogenation temperature up to 520 °C but decreases at a nitrogenation temperature of 560 °C (**Figure 6a**). This trend can be understood from the balance between the enhanced favorable visible light absorption and a simultaneous increase in the number of recombination centers of photogenerated charge carriers with a larger amount of nitrogen dopant. The Ti^{3+} defects generated by a high concentration of nitrogen dopant achieved at 560 °C, as illustrated in Figure 3,

act as recombination centers to impair the photoelectrochemical activity.

The photocurrent density (J_{photo}) generated by the illuminated photoanode can be depicted as follows:

$$J_{photo} = qg \frac{k_{tr}}{k_{tr} + k_{rec}}$$

where, q is the unit charge, g is the flux of holes into the surface, k_{tr} is the rate constant for hole transfer and k_{rec} is the rate constant for electron/hole recombination at the surface. k_{tr} is considered to be independent of the potential applied. k_{rec} is proportional to the electron concentration at the surface (n_{surf}) that decreases with the increase of band bending as follows.

$$n_{surf} = n_b \exp\left(\frac{-q\phi_{sc}}{k_B T}\right)$$

where, n_b is the electron (majority carrier) concentration in bulk, ϕ_{sc} is the band bending potential at the surface and increases with the increase of applied potential. Therefore, the photocurrent density increases with the increase of potential applied for each sample due to the reduction of k_{rec}. The increased photocurrent density at the fixed potential with the increase of nitrogenation temperature before 520 ^{o}C is mainly attributed to the improved absorption in visible light region that correspondingly increases the g value. Although further increasing nitrogenation temperature beyond 520 ^{o}C can increase visible light absorption for a larger g value, the k_{rec} value is also greatly improved as a result of the generation of the Ti^{3+} defects as deleterious recombination centers.

On the other hand, photoanodes of B/N-doped TiO_2 with different nitrogen contents show distinct photocurrent generation behaviors between the switching on and off of

light as highlighted in Fig. 6b. Compared to the flat step-like photocurrent response to the switching on and off of light in the photoanode of the pristine boron-doped TiO_2, the high nitrogen doping causes a striking jump of the photocurrent when the light is switched on as a result of the charging process.[34, 35] This striking jump is similar in all the different nitrogen-doped TiO_2 photoanodes. The stored charges in the TiO_2-440 and TiO_2-480 photoanodes are discharged by releasing cathodic current after the light irradiation is blocked, while no cathodic current was observed in the TiO_2-520, TiO_2-560 and TiO_2 photoanodes. This difference could be caused by the different electronic structures of doped TiO_2. Different from the samples with delocalized N 2*p* states, the localized nature of the N 2*p* states in the TiO_2-440 and TiO_2-480 samples limits the mobility of photogenerated holes in the material under visible light irradiation so that the slow release of the stored charges can contribute to the dark current.

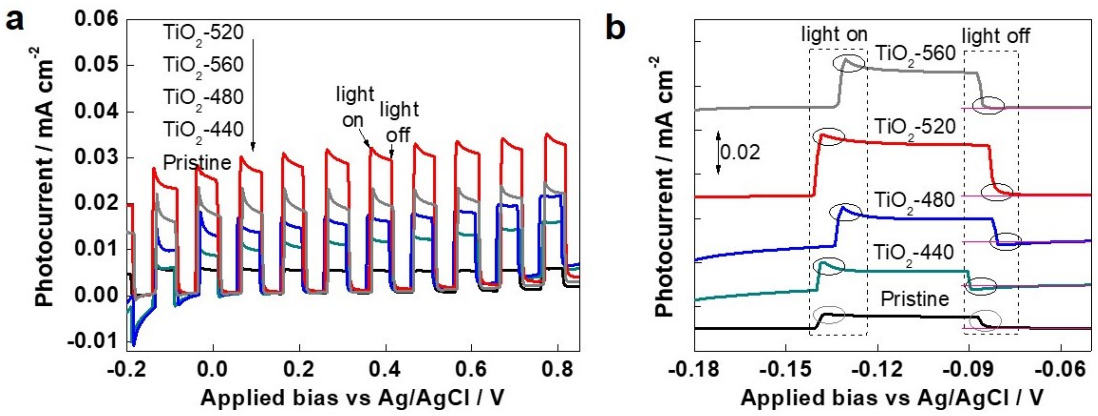

Figure 6 a, The applied bias dependent photoelectrochemical water oxidation current curve for photoanodes of B/N-doped TiO_2 microspheres prepared at different nitrogenation temperatures (440 ºC, 480 ºC, 520 ºC and 560 ºC) compared with that for a pristine TiO_2 sample under visible light irradiation ($\lambda > 420$ nm). **b,** the enlarged I-V

curve in the bias range -0.18 and -0.05 V showing one light-on and light-off cycle from Figure 6a. The scanning direction is from negative to positive bias.

It is useful to compare the dependence of the photoelectrochemical activity of the B/N-doped TiO_2 on the nitrogen concentration with that of the homogeneous nitrogen-doped $Cs_{0.68}Ti_{1.83}O_4$ and also nitrogen-doped TiO_2. Both the B/N-doped TiO_2 and homogeneous nitrogen-doped $Cs_{0.68}Ti_{1.83}O_4$ [29] show similar trends in that the activity increases with increased nitrogen concentration. In contrast, the activity of nitrogen-doped TiO_2 with a shoulder-like absorption band decreases with increased nitrogen concentration. [26] The reason for this trend is that the number of oxygen vacancies, which promote the recombination of electrons and holes, increases with the increase of nitrogen dopant. In the cases of homogeneous nitrogen-doped $Cs_{0.68}Ti_{1.83}O_4$ and B/N-doped TiO_2, the interstitial boron and cesium ions can compensate for the charge imbalance between O^{2-} and N^{3-} to suppress the formation of recombination centers.

The photoelectrochemical water oxidation activity in Figure 6 achieved with bare B/N-doped TiO_2 photoanodes is low, though the photocurrent density of the photoanode of doped TiO_2 with an optimized amount of born and nitrogen is about two times higher than that of the photoanode of the red TiO_2 with hydrogen filled oxygen vacancies[36]. It is anticipated that loading suitable co-catalysts for oxygen evolution reaction on B/N-doped TiO_2 can further improve activity and is to be conducted in future studies.

Discussion

A series of B/N-doped TiO_2 materials with different nitrogen concentrations was

prepared by annealing interstitial boron-doped TiO_2 microspheres with exposed {001} facets in gaseous ammonia at different temperatures (440, 480, 520 and 560 ^oC). The ratio of nitrogen dopant to titanium in TiO_2 gradually increased from 7.03 at% at 440 ^oC to 15.47 at% at 560 ^oC. An additional absorption band was formed that spanned the whole spectrum of visible light, and its absorbance increased with an increased nitrogen concentration. Particularly, as a consequence of bandgap narrowing, the sample obtained at 520 ^oC has the highest absorbance in visible light and no background absorption associated with defects. The photoelectrochemical water oxidation activity under visible light irradiation increases with an increase in the amount of nitrogen dopant before the formation of oxygen vacancies. The sample obtained at 520 ^oC gives the highest activity among the series of B/N doped anatase TiO_2 photocatalysts.

Experimental Section

Sample preparation: Interstitial boron-doped TiO_2 microspheres (around 95 wt% anatase and 5 wt% rutile) were prepared by the acid hydrolysis of a TiB_2 precursor according to a reported procedure.[27] Prior to nitrogen doping, they were heated at 600 ^oC for 2h in air to form a boron gradient in the outer layer of the microspheres. Subsequent heating at different temperatures (440, 480, 520 and 560 ^oC) in a gaseous ammonia atmosphere with a flux of 50 ml min^{-1} for 2 h was conducted to introduce different concentrations of nitrogen dopant. The resultant samples were denoted TiO_2-440, TiO_2-480, TiO_2-520 and TiO_2-560. All samples after further nitrogen doping remained the same crystal structure as indicated by X-ray diffraction patterns in **Figure S1**.

Characterization: The morphology and microstructures of the obtained TiO_2 samples were investigated by scanning (Nova NanoSEM 430) and transmission electron microscopy (FEI Tecnai-F30). X-ray diffraction patterns of the samples were obtained with a Rigaku diffractometer using Cu Kα irradiation (λ = 1.54056 Å). The chemical states and compositions of the samples were determined by X-ray photoelectron spectroscopy (Thermo Escalab 250, using a monochromatic Al Kα X-ray source). All binding energies were referred to the C 1s peak (284.8 eV) that arises from adventitious carbon. A UV-visible diffuse reflectance spectrophotometer (JASCO V-550) was used to record the optical absorption spectra of the samples in the region of 300 to 800 nm. Raman and Fourier transform infrared spectroscopies (Lab-Ram HR 800 & Bruker Tensor 27) were used to detect local structural variations in the samples.

Photoelectrochemical water oxidation measurements: Photoelectrochemical water oxidation measurements were conducted in a quartz cell with a conventional three-electrode system. The working, counter and reference electrodes were respectively a deposit of the prepared TiO_2, a Pt foil and Ag/AgCl. The electrolyte was a 0.2 M Na_2SO_4 aqueous solution. Light irradiation was under an AM 1.5 G illumination (Newport) with a density of 100 mW cm^{-2}. The illuminated area of the photoanode surface was 1 cm^2, and the scan rate was 10 mV s^{-1}. UV light was removed with a 420 nm cut-off glass filter.

Acknowledgements

The authors thank the Major Basic Research Program, Ministry of Science and Technology of China (2014CB239401), National Science Fund of China (Nos.

51422210, 21633009, 51629201, 51521091), the Key Research Program of Frontier Sciences CAS (QYZDB-SSW-JSC039) for the financial support. G.L. thanks Newton Advanced Fellowship.

Author Contributions

Liu G conceived the project and Cheng HM guided the project. Hong XX conducted experimental section together with Kang YY and Kang XD. Zhen C, Irvine JTS and Wang LZ analyzed PEC results. Yin LC contributed to electronic structure analysis. Liu G and Hong XX wrote the manuscript and all other authors revised the manuscript.

References

[1] Fujishima A and Honda K, Electrochemcial photolysis of water at a semiconductor electrode. *Nature* 1972, 238: 37.

[2] Zou ZG, Ye JH, Sayama K and Arakawa H., Direct splitting of water under visible light irradiation with an oxide semiconductor photocatalyst. *Nature* 2001, 414: 625.

[3] Wang XC et al. A metal-free polymeric photocatalyst for hydrogen production from water under visible light. *Nat. Mater.* 2009, 8: 76.

[4] Tada H, Mitsui T, Kiyonaga T, Akita T and Tanaka K, All-solid-state Z-scheme in CdS-Au-TiO_2 three-component nanojunction system. *Nat. Mater.* 2006, 5: 782.

[5] Kudo A and Miseki Y, Heterogeneous photocatalyst materials for water splitting. *Chem. Soc. Rev.* 2009, 38: 253.

[6] Yan H et al. Visible-light-driven hydrogen production with extremely high quantum efficiency on Pt-PdS/CdS photocatalyst. *J. Catal.* 2009, 266: 165.

[7] Hu S et al. Amorphous TiO_2 coatings stabilize Si, GaAs, and GaP photoanodes for efficient water oxidation. *Science* 2014, 344: 1005.

[8] Yang J, Wang D, Han H and Li C, Roles of Cocatalysts in Photocatalysis and Photoelectrocatalysis. *Acc. Chem. Res.* 2013, 46: 1900.

[9] Maeda K et al. Photocatalyst releasing hydrogen from water-Enhancing catalytic performance holds promise for hydrogen production by water splitting in sunlight.

Nature 2006, 440: 295.

[10] Wang Q et al. Scalable water splitting on particulate photocatalyst sheets with a solar-to-hydrogen energy conversion efficiency exceeding 1%. *Nat. Mater.* 2016, 15: 611.

[11] Pan C et al. A Complex Perovskite-Type Oxynitride: The First Photocatalyst for Water Splitting Operable at up to 600 nm. *Angew. Chem. Int. Ed.* 2015, 54: 2955.

[12] Zhang G, Liu G, Wang L and Irvine JTS, Inorganic perovskite photocatalysts for solar energy utilization. *Chem. Soc. Rev.* 2016, 45: 5951.

[13] Asahi R, Morikawa T, Ohwaki T, Aoki K and Taga Y, Visible-light photocatalysis in nitrogen-doped titanium oxides. *Science* 2001, 293: 269.

[14] Chen X, Liu L, Yu PY and Mao SS, Increasing Solar Absorption for Photocatalysis with Black Hydrogenated Titanium Dioxide Nanocrystals. *Science* 2011, 331, 746.

[15] Asahi R, Morikawa T, Irie H and Ohwaki T, Nitrogen-Doped Titanium Dioxide as Visible-Light-Sensitive Photocatalyst: Designs, Developments, and Prospects. *Chem. Rev.* 2014, 114: 9824.

[16] Kapilashrami M, Zhang Y, Liu YS, Hagfeldt A and Guo J, Probing the Optical Property and Electronic Structure of TiO_2 Nanomaterials for Renewable Energy Applications. *Chem. Rev.* 2014, 114, 9662.

[17] Zong X et al. Photocatalytic water oxidation on F, N co-doped TiO_2 with dominant exposed {001} facets under visible light. *Chem. Commun.* 2011, 47: 11742.

[18] Zhao W, Ma WH, Chen CC, Zhao JC and Shuai ZG, Efficient degradation of toxic organic pollutants with $Ni_2O_3/TiO_{2-x}B_x$ under visible irradiation. *J. Am. Chem. Soc.* 2004, 126: 4782.

[19] Sun Q et al. The Formation of Defect-Pairs for Highly Efficient Visible-Light Catalysts. *Adv. Mater.* 2017, 29: 1605123.

[20] Cheney CP et al. Origins of Electronic Band Gap Reduction in Cr/N Codoped TiO_2. *Phys. Rev. Lett.* 2014,112: 036404.

[21] Gai Y, Li J, Li SS, Xia JB and Wei SH, Design of Narrow-Gap TiO_2: A Passivated Codoping Approach for Enhanced Photoelectrochemical Activity. *Phys. Rev. Lett.* 2009, 102: 036402.

[22] Zhu W et al. Band Gap Narrowing of Titanium Oxide Semiconductors by Noncompensated Anion-Cation Codoping for Enhanced Visible-Light. *Phys. Rev. Lett.* 2009, 103: 226401.

[23] Liu G et al. Band-to-Band Visible-Light Photon Excitation and Photoactivity Induced by Homogeneous Nitrogen Doping in Layered Titanates. *Chem. Mater.* 2009, 21: 1266.

[24] Liu G, Wang L, Yang HG, Cheng HM and Lu GQ, Titania-based photocatalysts-crystal growth, doping and heterostructuring. *J. Mater. Chem.* 2010, 20: 831.

[25] Liu G et al. A red anatase TiO_2 photocatalyst for solar energy conversion. *Energy & Environ. Sci.* 2012, 5: 9603.

[26] Irie H, Watanabe Y and Hashimoto K, Nitrogen-concentration dependence on photocatalytic activity of $TiO_{2-x}N_x$ powders. *J. Phys. Chem. B* 2003, 107: 5483.

[27] Liu G et al. Heteroatom-Modulated Switching of Photocatalytic Hydrogen and Oxygen Evolution Preferences of Anatase TiO_2 Microspheres. *Adv. Funct. Mater.* 2012, 22: 3233.

[28] Yang HG et al. Anatase TiO_2 single crystals with a large percentage of reactive facets. *Nature* 2008, 453: 638.

[29] Liu G, Niu P, Wang L, Lu GQ, and Cheng HM, Achieving maximum photo-oxidation reactivity of $Cs_{0.68}Ti_{1.83}O_{4-x}N_x$ photocatalysts through valence band fine-tuning. *Catal. Sci. & Tech.* 2011, 1: 222.

[30] Ohsaka T, Izumi F and Fujiki Y, Raman-spectrum of anatase TiO_2. *J. Raman Spectroscopy* 1978, 7: 321.

[31] Balachandran U and Eror NG, Raman-spectra of titanium dioxide. *J. Solid State Chem.* 1982, 42: 276.

[32] Tanaka K and White JM, Characterization of species adsorbed on oxided and reduced anatase. *J. Phys. Chem.* 1982, 86: 4708.

[33] Sanchez E et al. Synthesis and characterization of sol-gel Pt/TiO_2 catalyst. *J. Solid State Chem.* 1996, 122: 309.

[34] Liu G et al. A Tantalum Nitride Photoanode Modified with a Hole-Storage Layer for Highly Stable Solar Water Splitting. *Angew. Chem. Int. Ed.* 2014, 53: 7295.

[35] Yang Y, Liu G, Irvine JTS and Cheng HM, Enhanced Photocatalytic H_2 Production in Core-Shell Engineered Rutile TiO_2. *Adv. Mater.* 2016, 28: 5850.

[36] Yang, YQ et al, An unusual strong visible-light absorption band in red anatase TiO_2 photocatalyst induced by atomic hydrogen-occupied oxygen vacancies, ***Adv. Mater.***, 2018, 1704479.

Xingxing Hong received his Bachelor's degree in Wuhan University in 2015. Now he is a PhD candidate in Institute of Metal Research, Chinese Academy of Sciences & University of Science and Technology of China. His crrent research is focusing on homogeneous doping of photocatalysts for visible light water splitting under the supervision of Professor Gang Liu and Professor Hui-Ming Cheng.

Gang Liu received his Bachelor degree in Materials Physics in Jilin University in 2003. He obtained his Ph.D. degree in Materials Science at Institute of Metal Research (IMR), Chinese Academy of Sciences (CAS) in 2009. Now he is a professor of IMR CAS. His main research interest is to develop photocatalytic materials for solar fuels.

B/N 掺杂富含{001}晶面锐钛矿 TiO_2 的最佳可见光光电催化水氧化活性研究

本文以锐钛矿 TiO_2 微米球光催化材料为研究对象，其表面主要由{001}晶面组成，间隙掺杂硼原子在微米球中呈浓度梯度分布，浓度最高点位于表面。通过对其在氨气气氛中不同温度下（440-560℃）进行热处理，可实现氮替代晶格氧的掺杂，氮掺杂原子的浓度随着热处理温度的增加从 7.03at%增加到 15.47at％。随着掺杂氮浓度的增加，所得掺杂 TiO_2 微米球的可见光吸收强度相应提高，进一步研究了所得掺杂 TiO_2 微米球的可见光光吸收、原子和电子结构与可见光光电催化水氧化活性的关联特性，发现在 520 ℃下所得氮掺杂 TiO_2 的可见光光电催化水氧化活性最大，该样品吸收光谱的显著特征是在可见光区吸光率高，且没有缺陷相关联背底吸收。